# Numerical Modeling of New Conceptions of 3D Printed Concrete Structures for Pumped Storage Hydropower

Eduardo de M. R. Fairbairn(✉), Larissa D. F. Santos, Marina B. Farias, and Oscar A. M. Reales

Civil Engineering Department/COPPE, The Federal University of Rio de Janeiro, Rio de Janeiro, Brazil
{eduardo,larissa.santos,marina.farias,oscar}@coc.ufrj.br

**Abstract.** This paper explores the possibilities of pumped storage hydropower (PSH), checking the possibilities of using new engineering tools such as 3D printing. The use of such technology for concrete has gained rapid development in recent years due to the advantages in structural optimization and economy with formwork in conventional construction. Practical engineering applications have proven the applicability of 3D printing in large-scale construction of building components, and compared to conventional manufacturing methods, this advanced technique has several advantages and offers almost unlimited potential for geometric complexities. We explore new design conceptions with the help of numerical modeling in two ways: (i) during the early ages considering the phenomena of hydration; (ii) after hardening of concrete verifying the integrity of the structure. The results indicated that numerical modeling can point to new solutions that will help address the challenges posed by greater sustainability in energy generation and storage in the 21st century.

**Keywords:** Pumped storage hydropower · 3D printing

## 1 Introduction

Pumped storage hydropower (PSH) plants, also called "water battery", are storage energy systems consisting of two water reservoirs, a tunnel connecting these reservoirs and a powerhouse with turbines-pumps and motor-generators. It represents one of the most sustainable, economical, and efficient solutions for energy storage, being an excellent alternative to store energy from intermittent sources such as wind and solar. To store energy, water is pumped from the lower reservoir to the upper reservoir. On the other hand, to generate energy, the water from the upper reservoir flows through the turbine towards the lower reservoir. To reduce system costs, whenever feasible, turbines and generators are also used as pumps and motors [1], as illustrated in Fig. 1 (taken from reference [2]). PSHs respond today for about 160 GW installed and 9,000GWh of energy storage across the globe [3]. The distribution of these plants (existing and planned) around the world are shown in Fig. 2 taken from reference [4].


P. Rossi and J.-L. Tailhan (Eds.): SSCS 2022, RILEM Bookseries 38, pp. 120–129, 2023.
https://doi.org/10.1007/978-3-031-07746-3_12

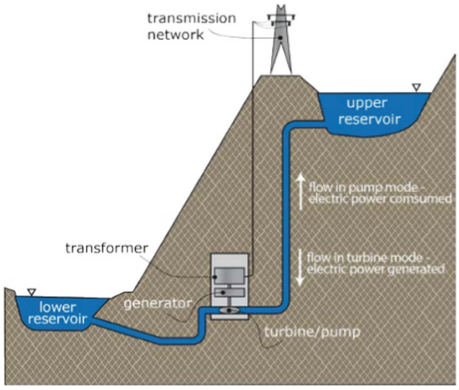


**Fig. 1.** Schematic of PSH ( taken from reference [2])

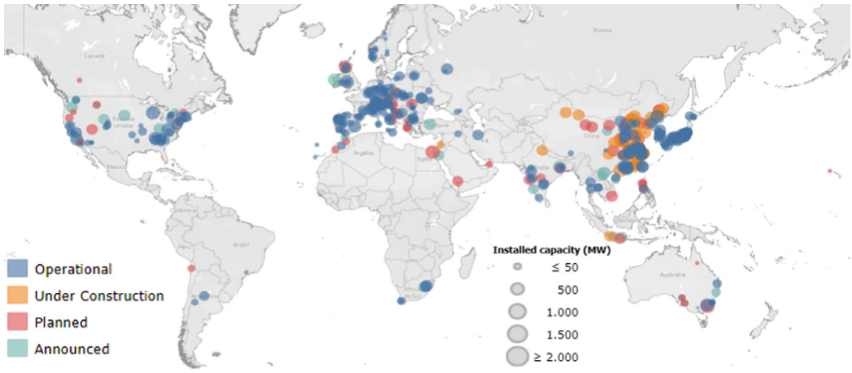


**Fig. 2.** Distribution of PSHs in the globe ( taken from reference [4])

It can be seen in Fig. 2 that, although PSHs are relatively new energy storage systems, they are already widely used in some regions of the world. On the contrary, in Brazil, although the hydroelectric potential of rivers is greatly explored, the use of PSHs is practically non-existent. However, the recent expansion of solar and wind energy generation is imposing the installation of "water batteries" to ensure the constancy of energy supply. In a recent comprehensive study [1] it was demonstrated that Brazil has great potential for building PSHs with different types of storage arrangements and cycles, which result in different benefits for the Brazilian Electricity Sector.

This paper explores the possibilities of this new type of hydroelectric development, checking the possibilities of using new engineering tools such as 3D printing. The use of such technology for concrete has gained rapid development in recent years due to the advantages in structural optimization and economy with formwork in conventional construction [5]. Practical engineering applications have proven the applicability of 3D printing in the large-scale construction of building components and compared to conventional manufacturing methods [6], this advanced technique has several advantages and offers almost unlimited potential for geometric complexities [7]. We explore the

potential of using 3D printing for the construction of PSH structures with the help of numerical modeling in two ways: (i) during the early ages considering the phenomena of hydration; (ii) after hardening of concrete verifying the possibility of introducing new design concepts. The results indicated that numerical modeling could point to new solutions that will help address the challenges posed by greater sustainability in energy generation and storage in the 21st century.

## 2 Theoretical Background

### 2.1 Modeling Parameters for 3D Printed Process

The process of 3D printing of cementitious material corresponds to the extrusion of this material through a tip with deposition of successive layers. The extruded material must be able to withstand its own weight and the weight of subsequent layers without significant deformations. This technique is capable of printing objects of great magnitude and complex geometries.

The physical model of a 3D printing that uses a cement matrix can be seen in Fig. 3. The model represents a 3D printing process through the deposition of successive layers and illustrates the parameters relevant to the printing process. Q represents the flow rate injected into the system, V represents the speed of the extruder nozzle and L represents the length to be expired. The total height is called Hm while the height of each layer is called h. Finally, W represents the thickness of the layer [8].

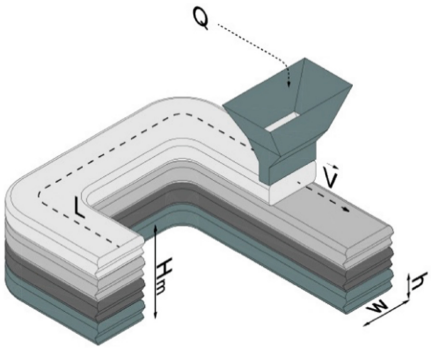


**Fig. 3.** Schematic of a layered extrusion process with concrete [8].

Some of the requirements that printable materials have is to verify the necessary structural strength that the building implies, given its geometric properties, and the correct consolidation of a layer before the deposition of the following, always maintaining a level of moisture that allows a good adhesion. Therefore, research carried out over time resulted in a series of equations that describe the behavior of fresh concrete submitted to the 3D printing process.

These materials, as well as any other cementitious materials, have the rheological behavior close to a Binghamian fluid, and two parameters are needed for their characterization: the flow stress and the plastic viscosity.

When the material is deposited, it displays an initial yield stress ($\tau_0$). Below this yield stress the material exhibits an elastic behavior. Due to thixotropic phenomena and cement hydration, the yield limit of the cement matrix increases over time. The initial yield limit, that is, the one measured as soon as the matrix has been mixed, will determine the maximum height ($h_{m,max}$) that each layer can have through the following equation [8].

$$h_{m,max} = \frac{\sigma_{0,0}\sqrt{3}}{\rho g} \tag{1}$$

Thixotropy of these types of materials and their ability to build an internal structure at rest is the key to most printing applications [9]. Thus, another important rheological property for the 3D printing process is thixotropic gain ($A_{thix}$). This corresponds to the rate of increase of yield limit over time, that is, the higher the thixotropic gain, the faster the cement will gain yield limit.

After the deposition of the layers, the rheological parameters evolve, and the experimental results show that, while the flow stress and the shear module increase, the deformation of the layers decrease, as a function of time [10, 11].

Since it is essential that the lower layer has sufficient flow limit to support its own weight beyond the weight of the top layer, the structural kinetics of the object must obey its size and its time window. The relationship between the minimum waiting time required between the layers ($t_{h,min}$) and the thixotropic gain is given by Eq. 2 [8].

$$t_{h,min} = \frac{\rho g h}{A_{thix}\sqrt{3}} \tag{2}$$

The maximum print speed ($V_{max}$) can be obtained by dividing the print length (L), which is the path to be traveled, by the minimum waiting time. Printing at speeds higher than maximum will lead to the structure collapsing.

Quick structuring is one of the benefits of 3D printing. However, there is a limit to this growth rate from the rheological point of view. High times between one layer and another can lead to so-called "cold joints" that lead to weak interface zones between these layers, and yet, the higher the thixotropy, the weaker the interface will also be [12].

Therefore, this will occur if a critical rest time between successive depositions is exceeded, thus defining a maximum layer time ($T_{max}$) given by Eq. 3 [9].

$$t_{h,max} = \frac{\sqrt{\frac{(\rho g h)^2}{12} + \left(\frac{2\mu_0 L}{h t_{h,max}}\right)^2}}{A_{thix}} \tag{3}$$

## 3 Experimental Program

Concrete was prepared with 600 kg/m$^3$ of Portland CPII-E cement, 1379 kg/m$^3$ of fine aggregate, with grain smaller than 0.2 mm, 259 kg/m$^3$ of water and 0.8% of superplasticizer per cement mass. Mixed for 2 min the solid compounds for complete homogenization, and another 8 min after added the rest of the materials for the action of the superplasticizer.

Rheology of the concrete was measured at room temperature using a rotational rheometer equipped with a 0.69 cm diameter and 1.176 cm height Vane spindle. Material was placed in a glass beaker, densified using a glass stirring rod, covered with plastic film and left to rest. The resting time ($t$) was defined as the time between the adding water and the beginning of the rheological testing. At the end of $t$, the vane spindle was introduced in the paste using the vertical guide of the rheometer, taking care of not disturbing the paste. The spindle was positioned in the center of the beaker at middle height. No pre-shearing was applied before the rheological measurements. Similar to [13] the author adopted rheology test for cementitious material.

Static yield stress ($\tau_{0;t}$) after a given $t$ was measured by shearing each sample from rest to a 0.2 $s^{-1}$ shear rate in 180 s. The value of $\tau_{0,t}$ was determined as the maximum stress recorded in the shear stress versus shearing time curve [14]. Tests at different resting times (0, 23, 45, 68 and 90 min) were used to characterize the structural buildup of the pastes. A fresh sample was used for each resting time to guarantee undisturbed conditions for each experiment [15].

The static yield stress data was used to characterize the structural buildup process of each formulation trough the rate of thixotropic build up ($A_{thix}$) [9]. The rate $A_{thix}$ was obtained by fitting the data to the linear equation below:

$$\tau_{0,t} = A_{thix}.t + \tau_{0,fit} \tag{4}$$

where $A_{thix}$ is the slope of the linear equation, t is the resting time and $\tau_{0;fit}$ is the static yield stress at $t = 0$, obtained from the intercept of the fitted equation.

### 3.1 Results

The static yield stress ($\tau_{0,t}$) versus time (t) for all studied mixtures are presented in Fig. 4. Linear equations of the form (4) were adjusted to these experimental results and are presented in the same figure. The parameters for construction of the 3D structure ($A_{thix}$, $\tau_{0,fit}$) were extracted from these linear equations.

An initial static yield stress of 2585 Pa and $A_{thix}$ of 0.85 Pa/s was obtained. Considering the density of 2162 kg/$m^3$ of the concrete and using the formulas (1) and (2), a layer of 20 cm height and 1 h of deposition time was adopted between the layers.

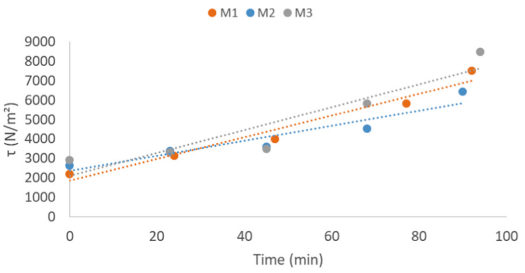


**Fig. 4.** Static yield stress ($\tau_{0;t}$) versus different mixtures and linear fits used to obtain $A_{thix}$ and $\tau_{0;fit}$ for concrete

## 4 Numerical Model

From previous studies and the analysis of three shapes commonly used in 3D printing, the lattice shape was chosen to be modeled in this work. Among the three shapes shown in Fig. 5, the structure with a square lattice interior has a slightly better result of stress levels, according to the study from reference [16], but the triangular truss shape is lighter and easier to execute, being the chosen shape to be studied in greater depth.

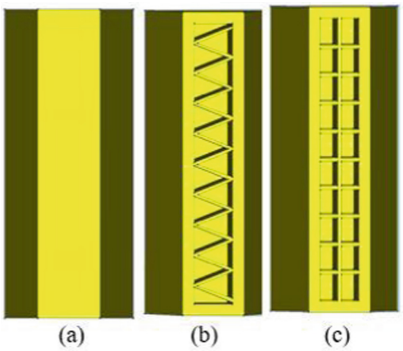


**Fig. 5.** Different dam wall shapes [16].

A numerical modeling was carried out using the finite element method and the design of the shape was made in the Autocad program to later be imported into the Diana FEA program, where the boundary conditions, material properties, mesh and, finally, the numerical analysis were established.

From the results of the tested concrete, a wall simulating a part of a wall of a PHS was modeled, built with 3D technology. This structure was simulated with 6 m high, 2.5 m thick and 6 m in length and it was divided into 30 layers with 20 cm in height each, as shown in Fig. 6.

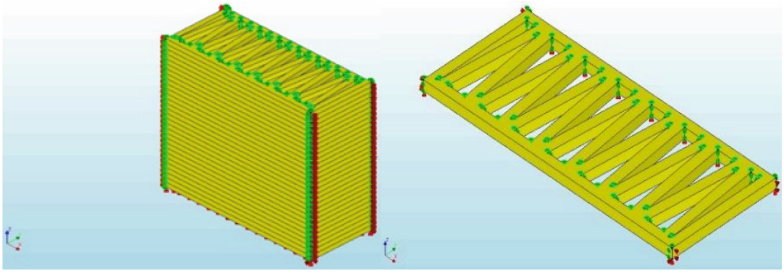

**Fig. 6.** Geometry of the numerical model

The model´s mesh, shown in Fig. 7, is formed by hexahedral elements with 10 cm of size. For the finite element analysis, quadratic elements were defined.

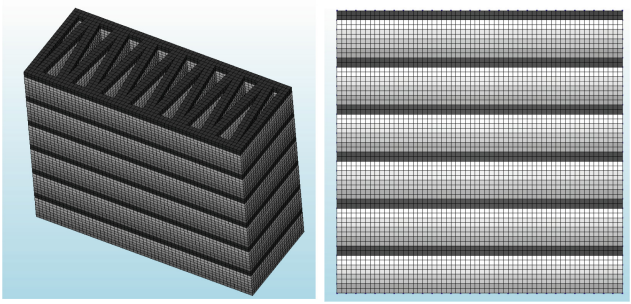

**Fig. 7.** Model's mesh

### 4.1 Numerical Modeling of the Structure in the Fresh State

The results were observed from the pouring of the first layer to the 16th layer, by limitations of the software and hardware, obtaining the highest possible degree of hydration, considering the placing temperature of 24 °C, constant ambient temperature of 22 ºC, height of the layer of 20 cm and interval of 1 h between the layers. The usual thermal properties of concrete estimated by Fairbairn [13], together with the tested thermal data, were considered, using conductivity of 4.0 W/mK and capacity of 2.5 x $10^6$ J/$m^3$K.

The boundary conditions considered the continuous wall in the direction of the longest length, heat flux between the layers, and concrete as an elastic material. The stresses are primarily influenced by the temperature field, and to a less degree by the dead load, while the effect of other loads was neglected.

**Results.** The result of the initial tension and tension increments due to the deposition of the layers both numerical and the experimental can be observed in Fig. 8. The setting process of the concrete starts 2:30 h after mixing, and ends at about 5 h, after which is considered as a hardened material.

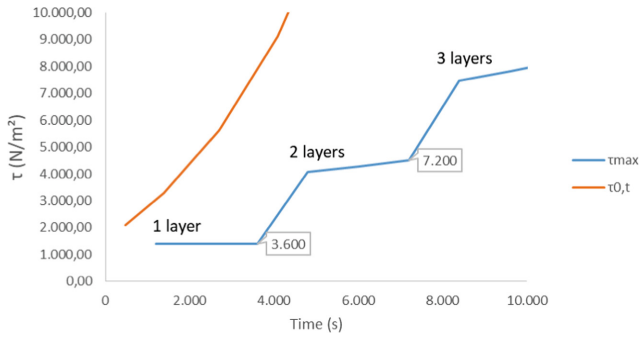


**Fig. 8.** Static yield stress (τ0,t) and maximum numerical shearing stress versus time

It can be seen in the above figure that the construction process is stable, given that the yield stress is always greater than the maximum shear stress during construction.

### 4.2 Numerical Modeling of the Structure in the Hardened State

As well as for the early age analysis, DIANA FEA was used to analyze the structure's performance at the hardened state. A structural nonlinear analysis of the walls was made to evaluate the stress distribution and integrity of the structure due to the acting forces, namely the dead weight and hydrostatic pressure. It is important to note that the program calculates the water pressure automatically, with the need to enter only the hydraulic head.

The following support restrictions were applied: the base was restricted in the x, y and z directions and the sides were restricted in the x direction. Between the layers, interface elements were used.

**Material Properties.** The material used was plain concrete and interface connections were applied between layers. the main properties of concrete are: young's modulus of 14 GPa, Poisson's rate of 0.3, mass density of 2062 kg/m$^3$, tensile strength of 3.0 MPa and a fracture energy ($G_f$) of 200 J/m. For the tensile behavior, the linear model was used with post-crack behavior based on fracture energy (linear-crack energy). for compression, the elastic model was used. For the interface material, the main properties are: normal and shear stiffness of 42 GPa, cohesion of 1.5 MPa, friction and dilatancy angle of 0.01 rad and tensile strength of 1.5 MPa. The interface opening model is the gapping model and the model for gap appearance is brittle.

**Crack Index.** To assess the capacity of the structure to resist the solicitant efforts, the crack index was used, which indicates how far the state of stresses is from the state of crack formation. This index is calculated by the ratio between the maximum principal stress and the tensile strength of concrete, as shown in Eq. (5) [17]:

$$F_{tu} = \frac{\sigma_1}{f_t} \tag{5}$$

where $\sigma_1$ is the maximum principal stress and $f_t$ is the concrete tensile strength.

**Results.** The maps of normal stresses ($S_1$), shear stresses ($T_{max}$) and crack index ($F_{tu}$) were obtained, as shown in Fig. 9. As expected, there was a concentration of tensile stress at the extremes of the edges and base of the walls. Figure 9 present the results for the side view (where the water pressure is acting) of the model.

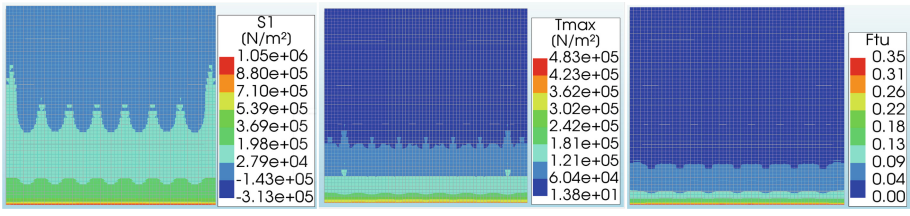


**Fig. 9.** Normal stress, shear stress and crack index maps at load step 1.0

To evaluate the behavior of the structure until failure, more load steps were taken, up to a load factor of 1.86, which multiplied by the water level would give a level of 11.16 m. From Fig. 10, it can be seen that there was a rupture between the first and second layers, evidencing that the structure reached stresses values greater than it can resist and, as consequence, there was a crack formation.

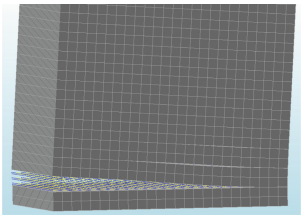

**Fig. 10.** Detail of crack between layers

## 5 Concluding Remarks

This paper presents an early analysis of an innovative design of structure to be used in new types of hydroelectric projects. The main idea is that a new type of hydroelectric plant is an interesting exploratory field for the development of innovative structural concepts that can make use of new technologies such as 3D construction. To this end, tools such as computer modeling using the finite element method are used, not only for hardened structures but also for the fresh concrete phase. The procedures presented here are still in an initial phase, but they intend to show the civil construction industry the advantages of using sophisticated simulation tools that may allow the development of new structural concepts.

## References

1. Brandão, R., Nivalde, D. C., Hunt, J.: The Viability of Reversible Power Plants in the National Interconnected System. ANEEL (2021). (in Portuguese)
2. Viadero, R.C., Singh, A., Rehbein, M.: Hydropower on the Mississipi River (2017)
3. Pump it up : Recommendations for urgent investment in pumped storage hydropower to back the clean energy transition. International Forum on Pumped Storage Hydropower Policy and Market Frameworks Working Group. Global Paper (2021)
4. Pumped Storage Tracking Tool: IHA (International Hydropower Association) (n.d.). https://professional.hydropower.org/page/map-pumped-storage-tracking-tool. Accessed 10 Mar 2022
5. Ngo, T.D., Kashani, A., Imbalzano, G., Nguyen, K.T.Q., Hui, D.: Additive manufacturing (3D printing): a review of materials, methods, applications and challenges. Compos. Part B: Eng. **143**(December 2017), 172–196 (2018). https://doi.org/10.1016/j.compositesb.2018.02.012
6. Zhang, J., Wang, J., Dong, S., Yu, X., Han, B.: A review of the current progress and application of 3D printed concrete. Compos. Part A: Appl. Sci. Manufact. **125**(April), 105533 (2019). https://doi.org/10.1016/j.compositesa.2019.105533

7. Paul, S.C., van Zijl, G.P.A.G., Gibson, I.: A review of 3D concrete printing systems and materials properties: current status and future research prospects. Rapid Prototyp. J. **24**(4), 784–798. https://doi.org/10.1108/RPJ-09-2016-0154
8. Wangler, T., et al.: Digital concrete: opportunities and challenges. RILEM Tech. Lett. **1**, 67 (2016). https://doi.org/10.21809/rilemtechlett.2016.16
9. Roussel, N.: A thixotropy model for fresh fluid concretes: theory, validation and applications. Cem. Concr. Res. **36**(10), 1797–1806 (2006). https://doi.org/10.1016/j.cemconres.2006.05.025
10. Wolfs, R.J.M., Bos, F.P., Salet, T.A.M.: Early age mechanical behaviour of 3D printed concrete: numerical modelling and experimental testing. Cem. Concr. Res. **106**(January), 103–116 (2018). https://doi.org/10.1016/j.cemconres.2018.02.001
11. Mettler, L.K., Wittel, F.K., Flatt, R.J., Herrmann, H.J.: Evolution of strength and failure of SCC during early hydration. Cem. Concr. Res. **89**, 288–296 (2016). https://doi.org/10.1016/j.cemconres.2016.09.004
12. Zareiyan, B., Khoshnevis, B.: Interlayer adhesion and strength of structures in contour crafting - effects of aggregate size, extrusion rate, and layer thickness. Autom. Constr. **81**(June), 112–121 (2017). https://doi.org/10.1016/j.autcon.2017.06.013
13. Fairbairn, E.M.R., Silvoso, M.M., Ribeiro, F.L.B., Toledo-Filho, R.D.: Determining the adiabatic temperature rise of concrete by inverse analysis: case study of a spillway gate pier. Eur. J. Environ. Civil Eng. **21**(3), 272–288 (2017). https://doi.org/10.1080/19648189.2015.1112843
14. Mendoza Reales, O.A., et al.: Influence of MWCNT/surfactant dispersions on the rheology of Portland cement pastes. Cem. Concr. Res. **107**(August 2017), 101–109 (2018). https://doi.org/10.1016/j.cemconres.2018.02.020
15. Mendoza Reales, O.A., Duda, P., Silva, E.C.C.M., Paiva, M.D.M., Filho, R.D.T.: Nanosilica particles as structural buildup agents for 3D printing with Portland cement pastes. Constr. Build. Mater. **219**, 91–100 (2019). https://doi.org/10.1016/j.conbuildmat.2019.05.174
16. de Farias, M.B., Fairbairn, E.M.R., Reales, O.A.M.: Numerical modeling of 3D-printed concrete dams designed for pumped-storage hydropower (2021)
17. Diana Fea, B.V.: DIANA finite element analysis user's manual. Release 10.5. (2021). Delft, the Netherlands